Multi-Directional Mechanofluorochromism of Acetyl Pyrenes and Pyrenyl Ynones

Yuichi Hirai, Lucie Laize-générat, Anna Wrona-piotrowicz, Anna Makal, Arnaud Brosseau, Laurent Michely, Davy-louis Versace, Clémence Allain, Rémi Métivier

ChemPhysChem

Chemistry Europe
European Chemical Societies Publishing

Accepted Article

Title: Multi-Directional Mechanofluorochromism of Acetyl Pyrenes and Pyrenyl Ynones

Authors: Yuichi Hirai, Lucie Laize-Générat, Anna Wrona-Piotrowicz, Janusz Zakrzewski, Anna Makal, Arnaud Brosseau, Laurent Michely, Davy-Louis Versace, Clémence Allain, and Rémi Métivier

To be cited as: *ChemPhysChem* 10.1002/cphc.202100294

Link to VoR: https://doi.org/10.1002/cphc.202100294

WILEY-VCH

Multi-Directional Mechanofluorochromism of Acetyl Pyrenes and Pyrenyl Ynones

Yuichi Hirai,[a]* Lucie Laize-Générat,[a] Anna Wrona-Piotrowicz,[b] Janusz Zakrzewski,[b] Anna Makal,[c] Arnaud Brosseau,[a] Laurent Michely,[d] Davy-Louis Versace,[d] Clémence Allain[a]* and Rémi Métivier[a]*

Abstract: A series of acetyl pyrenes and pyrenyl ynones with and without *tert*-butyl groups showed distinct mechanofluorochromism (MFC). Four pairs of polymorphic solids were found out of six compounds and interestingly, each of them showed hypsochromic, bathochromic or off-to-on MFC. The MFC properties were rationalized by categorizing the packing schemes into herringbone, sandwich, beta and gamma motifs depending on the relative contributions of C···C (or π-π) against C···H contacts. The bulky *tert*-butyl and trimethylsilyl groups served not only to reduce the number of aggregation patterns but also to prohibit the complete back reactions in solid state. Our results suggest that the simple pyrene derivatives may be promising candidates for a novel group of mechanically-sensitive materials.

Introduction

Solid-state luminescence of organic and organometallic compounds greatly depends on the molecular assembled structures, and luminescence intensity and/or color change triggered by mechanical stimuli such as crushing and grinding has been reported, generally denoted as mechanofluorochromism (MFC) or mechanochromic luminescence (MCL).[1][2][3] A series of gold(I) isocyanide complexes would be amongst the most well-known MCL-active group of compounds,[4][5][6] and organic-based MFC composed of rigid π-conjugated systems and mobile side groups has extensively been studied as well.[7][8][9] These MFC properties arise from the crystal-to-amorphous or crystal-to-crystal phase transitions accompanying the formation/destruction of metallophilic interactions, twisted/coplanar and monomer/excimer arrangement changes.

Organic compounds that exhibit aggregation-induced emission (AIE), charge transfer (CT) or polymorphism are promising candidates to host MFC due to the multiple accessible structures with orientation-dependent emission properties in aggregated states.[10][11][12] For example, an AIE-active 4H-pyran derivative was reported to form three polymorphs with distinct MFC properties that share the same molecular arrangement in ground form.[13] A small difference in chemical structures and packing motifs can also induce significant difference in mechanical responses, represented by *p*- and *m*-substituted tetraphenylethylene isomers with and without MFC.[14] The inversion of chromic directions was achieved by modifying the linkage positions of imidazole-tetraphenylethene compounds.[15] Most recently, *o*-, *m*- and *p*-brominated phenanthroimidazole-benzothiadiazole compounds were reported to give bicolor, one-way and back-and-forth MFC, respectively.[16] Considering the aggregation caused quenching (ACQ) of organic molecules which can limit their applications such as stress sensors and memory devices, it is important to focus on the fluorescent compounds in solid state as well as to control the chromic directions and the stability of deformed structures.

1-Acetylpyrene (**AP**) is a common simple molecule but has been reported as either emissive or non-emissive, which recently turned out to be caused by polymorphism.[17][18][19] Three crystal structures, so-called α-type, β-type and γ-type, were successfully determined with slight difference in lattice energy, resulting in distinct fluorescence properties depending on the molecular arrangements. It indicates that even a simple molecule like **AP** has potential to accommodate MFC properties, which is still challenging for small organic molecules. We recently reported that a series of fluorescent pyrene-derived amidophosphonates showed MFC in blue/green region, and the side groups (methyl, *i*-propyl, phenyl) were found to induce varied self-recovery processes in solid state depending on their rigidity.[20] A family of 14 different alkylpyrenes also demonstrated that the side alkyl chains could alter the solid-state molecular arrangements and corresponding emission colors and efficiencies without significant electronic effects.[21] Therefore, systematic study on pyrene-based MFC would provide a new library of mechano-responsive materials and knowledge about structure-property relationships. We here report the MFC of six acetyl pyrenes and pyrenyl ynones (Figure 1) including four pairs of polymorphs, and discuss the relationships between mechanical and photophysical properties on the basis of crystallography and spectroscopy.

[a] Dr. Y. Hirai, Ms. L. Laize-Générat Mr. A. Brosseau, Dr. R. Métivier, Dr. C. Allain
PPSM, CNRS, ENS Paris-Saclay
4 Avenue des Sciences 91190 Gif-sur-Yvette, France
E-mail: yuichi.hirai@ens-paris-saclay.fr, remi.metivier@ens-paris-saclay.fr, clemence.allain@ens-paris-saclay.fr
[b] Dr. A. Wrona-Piotrowicz, Prof. Dr. J. Zakrzewski
Department of Organic Chemistry, Faculty of Chemistry
University of Łódź
Tamka 12, 91-403 Łódź, Poland
[c] Dr. A. Makal
Biological and Chemical Research Center
University of Warsaw
Żwirki i Wigury 101, 02-089 Warszawa, PolandPoland
[d] Mr. L. Michely, Dr. D.-L. Versace
Institut de Chimie et des Matériaux Paris-Est, CNRS
94320 Thiais, France

Supporting information for this article is given via a link at the end of the document.

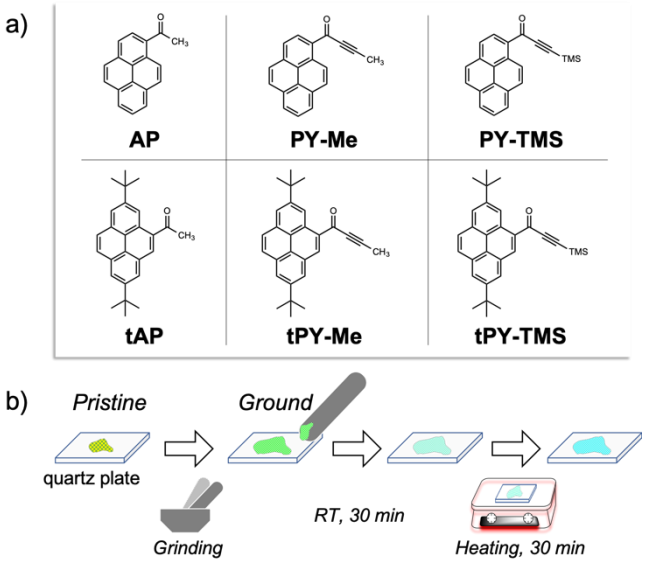

Figure 1. a) Chemical structures of target pyrene derivatives and b) schematic illustration of MFC measurement procedures (TMS = trimethylsilyl).

Results and Discussion

Acetylpyrenes and pyrenyl ynones with and without *tert*-butyl groups (Figure 1: **AP**,[19] **PY-Me**,[17] **PY-TMS**,[17] **tAP**,[22] **tPY-Me** and **tPY-TMS**) were prepared to investigate the MFC properties with different bulkiness and positions (1-substituted or 2,7-di-*tert*-butyl + 4-substituted pyrenes) based on the reported procedures. We first focused on the simplest compound **AP**. The non-emissive thin plate and green fluorescent block crystals were obtained from ethanol and dichloromethane solutions, respectively. According to the simulated powder X-ray diffraction (PXRD) patterns using the crystal information files (CIF),[19] the obtained PXRD patterns were assigned to be α type (space group Cc: **AP** (dark)) and γ type (space group $P2_1$: **AP** (green)), while β type (space group $P2_1/c$: **AP** (weak-green)) was not isolated in this study (see Supporting Information Figure S1a). The characteristic peaks of **AP** (dark) at 2θ = 6.1, 12.2, 18.2 and 30.6° correspond to the Miller indices (h k l) = (2 0 0), (4 0 0), (6 0 0) and (10 0 0), and those of **AP** (green) at 2θ = 11.8, 15.2, 29.4 and ~40° are assigned to be (0 0 3), (0 1 3), (3 1 3) and (3 3 3) planes, respectively. Since the thermodynamic stability of polymorphs increases with their crystal density,[23] relatively lower density of **AP** (weak-green) may be responsible for the difficulty to isolate it in the present study (Figure 2a, d_{dark} = 1.364 > d_{green} = 1.349 > $d_{weak\text{-}green}$ = 1.336 g cm^{-3}).

Upon mechanical grinding using a mortar and a pestle, we confirmed off-to-on emission intensity change of **AP** (dark) and hypsochromic spectral shift of **AP** (green), respectively (Figure 2b). Since the green fluorescence from the ground **AP** (dark) immediately disappeared and turned back to the original non-emissive state, we followed the solid-state back reactions to consider the possible molecular rearrangement. Room temperature was enough to induce the spontaneous back reaction and the additional heating at 50°C for 30 minutes did not give any notable change. On the other hand, **AP** (green) does not show any back reaction and the emission spectrum remains at the same position even after heating at 50°C. Mechanical stimulation applied on **AP** (green) triggers less pronounced changes in the fluorescence properties than for **AP** (dark), and the small hypsochromic shift indicates the decreased intermolecular interactions in the ground form.

In order to provide deeper insights into the MFC properties, time-resolved fluorescence measurements were performed for pristine and ground forms at three distinct emission wavelengths. Since each fluorescence decay measurement takes several minutes, the fast back reaction at room temperature may have influence on the detected signals. We here decided to select a sum of two to four discrete exponentials to fit the obtained decay curves (see Supporting Information Table S1 for full sets of data). The large contribution of the longest lifetime component at longer emission wavelength (τ_1 = 25 ns) of **AP** (dark) after grinding would be reasoned by the formation of aggregates or dimers in the ground state since it is not accompanied by rise time components. The small fractions of short-τ components (≦ 2.2 ns) that are more dominant in the blue region also indicate the existence of a limited fraction of monomeric species, which is compatible with the spectral profiles that display a main broad band in longer wavelength and monomeric shoulder peaks at shorter wavelength. On the other hand, a much longer decay-time component (≧ 40 ns) dominates almost all of the emission intensity of pristine **AP** (green) (f ≧ 0.99), and the mechanical grinding slightly decreases the degree of contribution (f = 0.92-0.97). It is therefore interpreted as the characteristic π-π dimeric species of **AP** (green) which are deformed under the condition of grinding, while **AP** (dark) temporarily forms aggregates with short intermolecular contacts which can enhance the solid-state fluorescence,[18] followed by the fast relaxation to the original non-emissive form. MFC of **AP** is then based on discrete structural deformation of each polymorph and mechanically-induced phase transitions between dark and green forms would not occur in this case (Figure 2c). The previous study also supports the comparable thermodynamic stability of **AP** (dark) and **AP** (green) and the lack of phase transitions between them.[19] Thus, the small difference in molecular packing motifs induces a large difference in the solid-state fluorescence and their mechanical response.

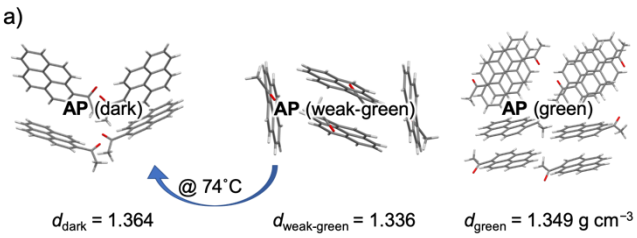

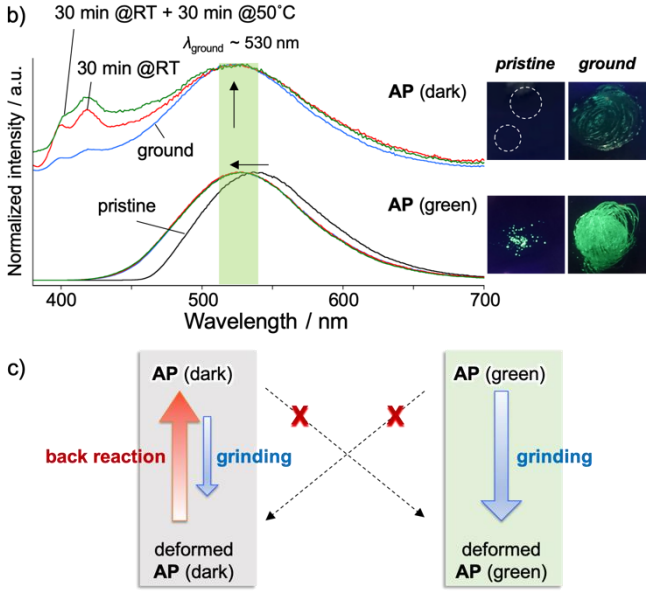

Figure 2. a) Crystal packing structures of **AP** (dark), **AP** (weak-green) and **AP** (green).[19] b) Solid-state emission spectra of **AP** (dark) and **AP** (green) (black: pristine, blue: ground, red: 30 min after grinding at RT, green: another 30 min at 50˚C, λ_{ex} = 360 nm) and pictures of pristine/ground forms under UV irradiation λ_{ex} = 365 nm (white dotted circle shows non-emissive plate crystals of **AP** (dark), arrows show the chromic directions of MFC). c) A schematic diagram of MFC in **AP**.

In the case of 4-acetylpyrene with *tert*-butyl groups in 2,7-positions (**tAP**), two polymorphic crystals were obtained; one is non-emissive and the other shows strong green fluorescence (Figure 3a). According to the single crystal X-ray analysis, the former one belongs to the monoclinic system, space group $P2_1$ (**tAP** (dark)), whereas the latter one belongs to the orthorhombic system, space group *Aea*2 (**tAP** (green)). The crystallographic parameters are summarized in Table S3 in Supporting Information. The correlation between molecular arrangements and fluorescence intensity of pristine solid samples is quite similar to those of **AP**. In particular, the steric hindrance of *tert*-butyl groups in **tAP** (green) is avoided by rotating the pyrene unit, resulting in a columnar π-π stacking ($d_{π-π}$ ~ 3.5 Å) along *c*-axis. The detailed intermolecular interactions were investigated based on Hirshfeld surface with shape index[24][25] and fingerprint plots[26] (Figures 3b and 3c), which is especially powerful to compare the different contributions of interactions in polymorphic organic compounds.[27] The characteristic circular arrangement of red and blue triangles on the shape index surface indicates the complementary patches due to the alternate twisted molecules in a columnar packing of **tAP** (green), while **tAP** (dark) without face-to-face contacts does not show these contributions (Hirshfeld surfaces with shape index of **AP** were shown in Figure S2 for comparison). The red-green-blue coloring schemes of fingerprint plots (red/blue spots: contacts shorter/longer than vdW separations) also visualized the difference of distributions and contributions of each contacts in **tAP**. The C···C contact of **tAP** (green) distributing at (d_i, d_e) ~ 1.8 Å represents the typical π-π stacking of aromatic hydrocarbons, whereas C···H and H···H contacts dominate more than 90% of the surface area of **tAP** (dark) with negligibly small contribution of C···C contact (0.5%).

As shown in Figure 3a, a pair of off-to-on and hypsochromic MFC was observed for **tAP** (dark) and **tAP** (green), respectively, in line with the behavior described for **AP**. Since both polymorphs didn't show significant back reactions either at room temperature or at 50˚C, a metastable state would lie between **tAP** (dark) with newly created intermolecular interactions and **tAP** (green) with dislocated conformers. The ground forms of **tAP** (dark) and **tAP** (green) showed quite similar emission spectral shapes (λ_{em} ~ 500 nm) and fluorescence decay-times (τ_1 = 19-21, τ_2 = 8.4-11, τ_3 = 1.3-2.5, τ_4 = 0.13-0.17 ns, see Figure S3b in Supporting Information for overlaid decay profiles). The short-τ component of ground **tAP** (green) in shorter wavelength with slight contribution corresponds to the appearance of an emission band at around 420 nm, which may correspond to a small fraction of monomeric emission.

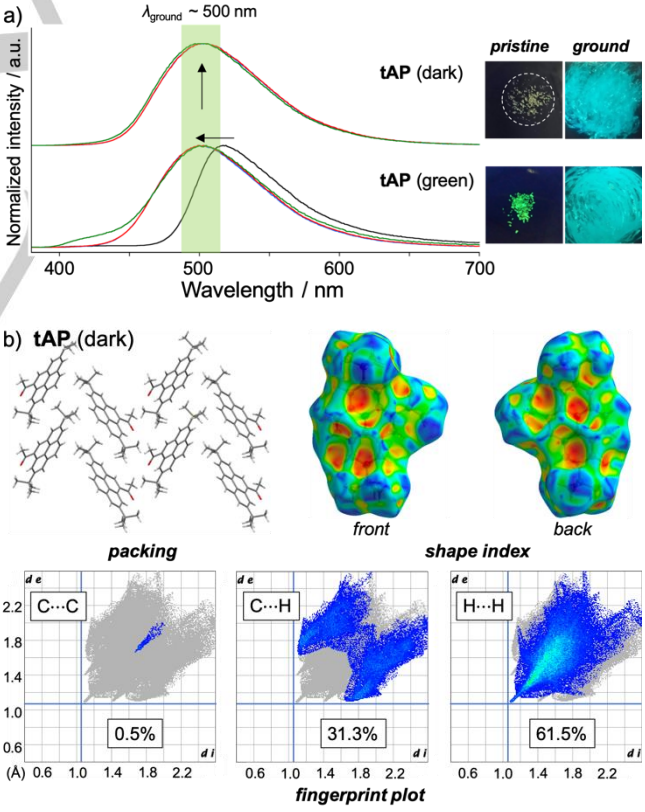

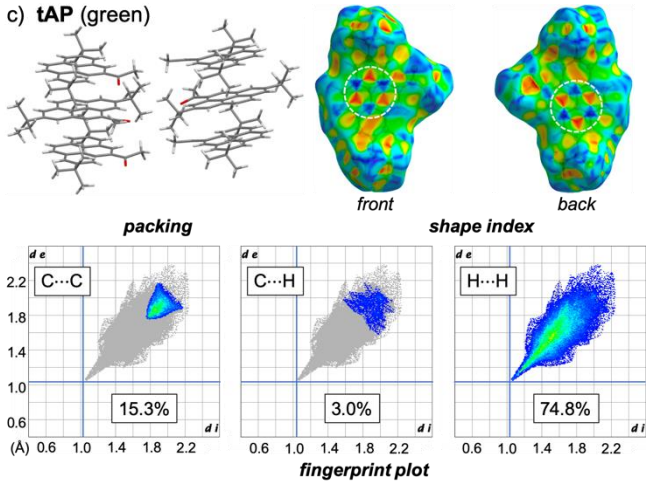

Figure 3. a) Solid-state emission spectra of **tAP** (black: pristine, blue: ground, red: 30 min after grinding at RT, green: another 30 min at 50˚C, λ_{ex} = 360 nm) and pictures of pristine/ground forms under UV irradiation λ_{ex} = 365 nm (white dotted circle shows non-emissive crystalline powder of **tAP** (dark), arrows show the chromic directions of MFC). Crystal packing structures, front/back views of the Hirshfeld surfaces with shape index and fingerprint plots for specific pairs of atom-types of b) **tAP** (dark) and c) **tAP** (green) (grey shadow: outline of the complete fingerprint plot, d_i and d_e: distances from the Hirshfeld surfaces to the nearest nucleus inside and outside the surface, respectively).

Finally, a series of pyrenyl ynones with and without *tert*-butyl groups (**PY-Me**, **tPY-Me**, **PY-TMS** and **tPY-TMS**) were investigated. We found two emissive polymorphs of **PY-Me** (Figure 4a, yellow form at 530 nm and orange form at 600 nm, respectively). According to the single crystal X-ray and PXRD analysis of **PY-Me** (orange), we confirmed that the previously reported crystal structure[17] was that of **PY-Me** (orange) of this study (see Supporting Information Figures S4-S6). Makal *et al.* also described the orange emission (λ_{em} ~ 597 nm) from a single crystal with infinite π-stacks in [100] direction which showed red-shifted emission under high isotropic pressure applied using a diamond anvil cell.[28] Although single crystals were not obtained for **PY-Me** (yellow), the reported photophysical properties of yellow-emissive powder (λ_{em} ~ 530 nm)[17] also indicates the face-to-face packing of pyrene motifs in the crystal lattice. Therefore, both **PY-Me** polymorphs are considered to form π-π stacking motifs but with different contributions, larger for the orange form than for the yellow form, which would affect their mechanical sensitivity. Indeed, a large bathochromic shift (Δ_{shift} ~ 50 nm) was observed for **PY-Me** (yellow), while **PY-Me** (orange) showed a hypsochromic shift, and no back reaction was noticed for both polymorphs, even after heating at 50˚C. The similar decay profiles in ground forms for both polymorphs (see Figure S3c in Supporting Information) and the absence of back reaction implies the existence of a metastable state of **PY-Me** as in the case of **tAP**.

Besides the previously reported yellow-emissive form of **PY-TMS**[17] (**PY-TMS** (yellow) with λ_{em} = 560 nm), a green-emissive polymorph was newly found (**PY-TMS** (green) with λ_{em} = 525 nm), and two distinct phases were recognized from PXRD patterns (see Figure S7 in Supporting Information). Unlike other compounds, **PY-TMS** (green and yellow) displayed a pair of bathochromic/hypsochromic MFC with back/forward reactions. **PY-TMS** (green) exhibited red-shifted fluorescence spectrum in ground form (λ_{em} ~ 560 nm), which was similar to that of pristine **PY-TMS** (yellow). The spontaneous back reaction was observed at room temperature, and the original green fluorescence was mostly recovered after heating at 50˚C. On the other hand, **PY-TMS** (yellow) showed blue-shifted fluorescence in ground form, and the spectrum shifted forward, towards shorter wavelengths, in 30 min at room temperature. Instead of recovering the original fluorescence of **PY-TMS** (yellow), further blue-shifted spectral profile appeared after heating at 50˚C, which was more bluish than that of pristine **PY-TMS** (green). As is the same for **AP**, each polymorph of **PY-TMS** undergoes MFC with distinct ground forms. The spectroscopy of molten samples supports the possible differences between "amorphous solids" that can be reached by mechanical grinding and by rapid-cooling after melting (see Supporting Information Figure S8). Since **PY-Me** and **PY-TMS** form two distinct emissive polymorphs with a pair of bathochromic and hypsochromic MFC, we systematically compared the fractions of intensity of each fluorescence decay-time component ($\tau_1 > \tau_2 > \tau_3 > \tau_4$) at each centered emission wavelength for pristine and ground forms. Figure 4b demonstrates that a polymorph with longer-λ_{em} always decreases its contribution of long τ-components ($\tau_1 + \tau_2$) and increases its short τ-components ($\tau_3 + \tau_4$) under mechanical stress (grinding), which indicates the dislocation of face-to-face dimers/excimers. Conversely, the corresponding shorter-λ_{em} polymorph exhibits the complementary tendency, and it demonstrates the partial formation of aggregated conformations. The differential scanning calorimetric analyses also showed the different thermodynamic properties between polymorphs (see Table S4 and Appendix 2 in Supporting Information for the list of observed temperatures and thermograms).

By introducing *tert*-butyl groups, a non-emissive solid (**tPY-Me**) was obtained, which is similar to that of **tAP** (dark). Although two types of non-emissive single crystals were found for **tPY-Me** (space groups $P2_1/n$ and $P2_1/c$), powder XRD patterns that belong to $P2_1/c$ phase were not identified in the pristine sample (see Table S3 and Figure S9 in Supporting Information). Then, the optical and mechanical properties of **tPY-Me** would be dominated by $P2_1/n$ phase, which is the one considered in the following discussion. The distances between centroids of pyrene motifs obtained by single crystal XRD analysis (Figure 4c) indicate that the *tert*-butyl groups reduce the overlapping of π-aromatic surfaces even they locate parallel in a short distance ($d_{\pi-\pi}$ = 3.36 and 3.32 Å for **PY-Me** and **tPY-Me**, respectively), unless the steric volume of the side groups is small enough to allow the head-to-tail or twisted stacking. The bulkiest pyrenyl ynone (**tPY-TMS**) didn't give polymorphs, and **tPY-Me** and **tPY-TMS** showed off-to-on and bathochromic MFC, respectively. The aggregated packing of ground **tPY-Me** and **tPY-TMS** are indicated by the broad spectral profiles and the largest contribution of the longest decay-time components (τ_1 = 16-18 ns). After mechanical stimulation, the solid-state back reaction at room temperature was slightly faster for **tPY-TMS** than for **tPY-**

Me, and significantly accelerated under the condition of heating at 50˚C only for **tPY-Me**. The MFC property of **tPY-TMS** with bathochromic shift and back reaction at room temperature and at 50˚C is comparable to that of **PY-TMS** (green). The steric structures of TMS [-Si(CH_3)$_3$] and *tert*-butyl [-C(CH_3)$_3$] groups are quite similar, and a TMS linked with a triple bond would be bulky and rigid enough to prevent the complete molecular rearrangement.

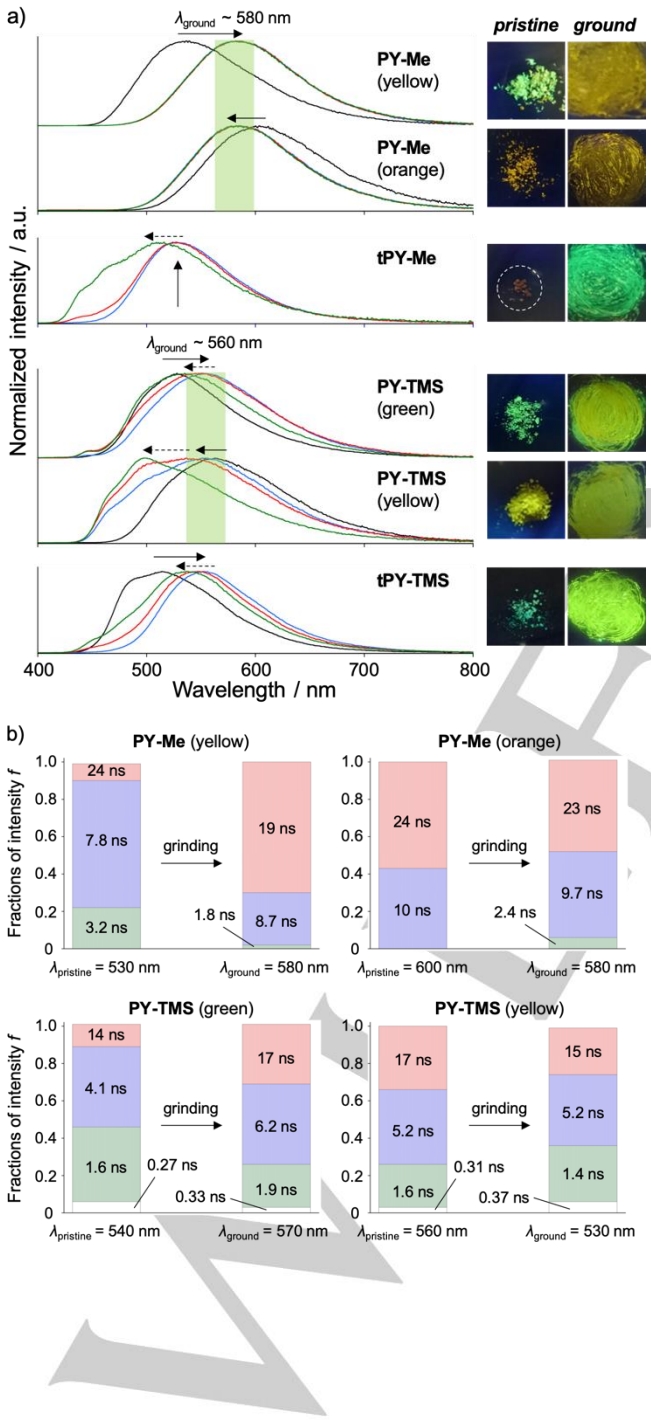

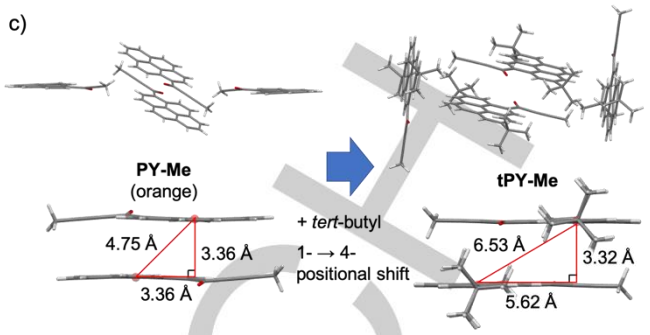

Figure 4. a) Solid-state emission spectra of pyrenyl ynones (black: pristine, blue: ground, red: 30 min after grinding at RT, green: another 30 min at 50˚C, λ_{ex} = 360 nm, solid and dotted arrows inset show the chromic directions of MFC and back/forward reactions) and pictures of pristine/ground forms under UV irradiation λ_{ex} = 365 nm (white dotted circle shows non-emissive powder of **tPY-Me**, see Figure S10 in SI for full sets of excitation spectra), b) fractions of intensity *f* of **PY-Me** (top) and **PY-TMS** (bottom) in pristine and ground forms (τ_1-τ_4: red, blue, green and white columns, respectively) and c) packing scheme of **PY-Me** (orange) and **tPY-Me** (the length of hypotenuse of a right triangle shows the distance between centroids of pyrene motif).

Table 1. Summary of MFC properties of studied compounds and results obtained from fingerprint plot analysis (if available).

Sample	Pristine fl. color	MFC type ($\Delta\lambda_{MFC}$)[a]	ρ indicator[b] (%C···H/%C···C)	Motif (observed)
AP (dark)	dark	off-to-on	24	herringbone
AP (green)	green	hypsochromic (−13 nm)	3.5	sandwich
tAP (dark)	dark	off-to-on	63	herringbone
tAP (green)	green	hypsochromic (−27 nm)	0.20	β
PY-Me (yellow)	yellow	bathochromic (+36 nm)	–	–
PY-Me (orange)	orange	hypsochromic (−21 nm)	1.1	β-γ
PY-TMS (green)	green	bathochromic (+18 nm)	–	–
PY-TMS (yellow)	yellow	hypsochromic (−22 nm)	–	–
tPY-Me	dark	off-to-on	5.7	herringbone
tPY-TMS	green	bathochromic (+36 nm)	–	–

[a] $\Delta\lambda_{MFC} = \lambda_{mean,ground} - \lambda_{mean,pristine}$. [b] The ρ indicator of π-stacking extent in the three crystal forms (β 0.46 < ρ < 1.0, γ 1.2 < ρ < 2.7, sandwich 3.2 < ρ < 4.0 and herringbone ρ > 4.5).[27]

For summary, we estimated the ρ indicators[27] that are dimensionless quantities estimated from the contribution of C···H and C···C (or π-π) contacts to categorize the packing motifs into four models, namely β, γ, sandwich and herringbone (Figure 5, see Supporting Information Table S5 for discrete contributions). The molecules with π-π stacking conformers (β, γ and sandwich motifs) give small hypsochromic shift in emission profiles, while the herringbone structure gives bathochromic shift upon grinding, accompanying off-to-on emission intensity change. The former is caused by the reduced intermolecular interactions in ground form than in pristine one, and the latter is due to the increased intermolecular interactions with partial π-π aggregates (*e.g.* herringbone-to-*quasi*-sandwich packing change). Similar effect was demonstrated by a pair of hypsochromic and bathochromic MFC in gold(I) complexes with suppressed and enhanced π-π stacking interactions upon grinding.[29] The destruction of hydrogen bonds in hypsochromic MFC system was also confirmed by the disappearance of N-H stretching absorption bands in dimethoxynaphthalene-based compounds.[30] On the other hand, bulky side groups reduce the relative contribution of π-aromatic planes to the entire molecular surfaces and the π-π interactions are less likely to be formed under crystallization, which leads to the herringbone motif with bathochromic MFC. Indeed, many of the reported MFC-active pyrene derivatives bear bulky substituents such as dioxaboron,[31] alkanoylamine,[32] and tri-substituted phosphines,[33] and bathochromically shifted emission upon grinding can be reasoned by the same manner.

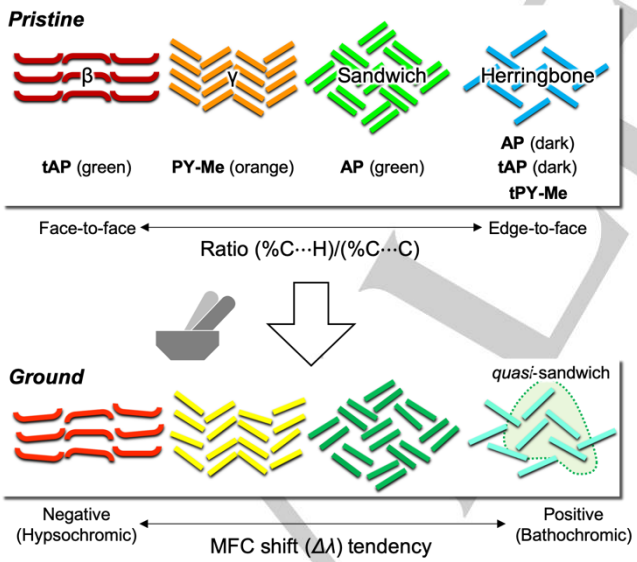

Figure 5. Diagrammatic representation of β, γ, sandwich and herringbone packing motifs in pristine/ground forms (solid and dotted arrows show hypsochromic and bathochromic shift, respectively).

Conclusions

A series of acetyl pyrenes and pyrenyl ynones with and without *tert*-butyl groups were prepared. Every compound demonstrated hypsochromic, bathochromic or off-to-on MFC upon grinding. It appears that the molecular packing structures drove not only the direction of color change under mechanical stress but also the corresponding back and forward spontaneous reactions in solid state after the stimulation. These photophysical properties were consistently rationalized by considering the crystal packing motifs, spectral profiles and emission decay-time components. Compounds with less sterically-hindered side groups tend to show more diverse molecular arrangements such as twisted/head-to-tail/shifted π-π and edge-to-face CH-π stacking, and the ratios of contribution between face-to-face and edge-to-face interactions certainly impact on the mechanical properties. The existence of unknown polymorphs with quite close lattice energy is still possible for the investigated compounds, which is difficult to find either theoretically or experimentally. The synthetic diversity of pyrene derivatives with small differences in steric structures and solid-state fluorescence are also helpful to find a clue to these crystal engineering issues. Since many of the MFC research were not devoted to the self-recovery process, further study on the detailed solid-state properties would lead to the development of new mechano-responsive materials with controlled back reactions.

Experimental Section

AP,[19] **PY-Me**,[17] **PY-TMS**[17] and **tAP**[22] were prepared following the earlier published procedure.

Preparation of 1-(2,7-di-tert-butylpyren-4-yl)but-2-yn-1-one (**tPY-Me**) and *1-(2,7-di-tert-butylpyren-4-yl)-3-(trimethylsilyl)prop-2-yn-1-one* (**tPY-TMS**): 2,7-di-*tert*-butylpyrene (314.5 mg, 1 mmol) and TfOH (1.1 mmol, 97 μL) were added to a solution of carboxylic acid (2-butynoic acid or 3-(trimethylsilyl)propiolic acid, 1.1 mmol) and TFAA (1 mmol, 139 μL) in 10 ml of anhydrous DCM at 0 °C. After 5 min the mixture was allowed to warm up to room temperature and it was stirred for 1h. After this time the reaction mixture was poured into water (50 mL) and extracted several times with dichloromethane. The combined extracts were dried over anhydrous Na_2SO_4 and evaporated to dryness. The crude product was purified by column chromatography (silica gel/ petroleum ether/ethyl acetate (95/5, v/v)).

tPY-Me. Yellow powder (346 mg, 91%); ^{1}H NMR (600 MHz, $CDCl_3$) δ 9.66 (d, J = 1.8 Hz, 1H), 9.17 (s, 1H), 8.36 (d, J = 1.8 Hz, 1H), 8.32 (d, J = 1.8 Hz, 1H), 8.25 (d, J = 1.8 Hz, 1H), 8.05 (d, J = 9.0 Hz, 1H), 8.01 (d, J = 9.0 Hz, 1H), 2.27 (s, 3H), 1.61 (s, 9H), 1.60 (s, 9H); ^{13}C{^{1}H} NMR (151 MHz, $CDCl_3$) δ 180.2, 149.9, 149.1, 138.8, 132.6, 130.8, 130.7, 128.9, 128.4, 127.2, 126.6, 125.4, 124.5, 124.3, 123.5, 123.1, 122.1, 122.0, 90.7, 80.7, 35.6, 35.2, 31.9, 31.9, 4.5; Anal. calcd. for $C_{28}H_{28}O$: C, 88.38; H, 7.42; found: C, 88.47; H, 7.33.

tPY-TMS. Yellow powder (382 mg, 87%); ^{1}H NMR (600 MHz, $CDCl_3$) δ 9.67 (d, J = 1.8 Hz, 1H), 9.21 (s, 1H), 8.34 (s, 2H), 8.26 (d, J = 1.8 Hz, 1H), 8.05 (d, J = 9.0 Hz, 1H), 8.01 (d, J = 9.0 Hz, 1H), 1.63 (s, 9H), 1.62 (s, 9H), 0.43 (s, 9H); ^{13}C{^{1}H} NMR (151 MHz, $CDCl_3$) δ 179.7, 149.9, 149.1, 139.4, 132.2, 130.8, 130.7, 128.7, 128.4, 127.1, 126.53, 125.71, 124.63, 124.3, 123.4, 123.2, 122.0, 102.6, 98.6, 35.6, 35.2, 31.8, -0.51; Anal. calcd. for $C_{30}H_{34}OSi$: C, 82.14; H, 7.81; found: C, 82.07; H, 7.91.

Optical Measurements: Emission and excitation spectra of pristine powder samples were recorded on a HORIBA Jobin-Yvon Fluorolog FL3-221 spectrometer using a short path length optical quartz cell (20/C/Q/0.2, Starna), and the spectra were corrected for the response of the detector system. The pristine powder was ground using an agate mortar, and the resulting amorphous solid adhered on a pestle surface was immediately transferred to a quartz plate to record the spectra and minimize the effect of back reaction at room temperature. Fluorescence decay profiles were obtained by time-correlated single-photon counting (TCSPC) method with titanium:sapphire laser (Tsunami, Spectra-Physics) pumped by a doubled Nd:YVO_4 laser (Millennia Xs, Spectra-Physics). Light pulses at 720 nm was selected by an acousto-optic crystal at a repetition rate of 0.8 MHz, and then doubled at 360 nm by nonlinear crystals. Fluorescence photons were detected at 90˚ through a polarizer at the magic angle and monochromator, by means of a Hamamatsu MCP R3809U photomultiplier, connected to a SPC-630 TCSPC module from Becker&Hickl. The instrumental response function was recorded before each decay measurement with a fwhm (full width half maximum) of 860 ps. The fluorescence data were analyzed using the Globals software package developed at the Laboratory for Fluorescence Dynamics at the University of California, which includes reconvolution analysis and global non-linear least-squares minimization method.

Crystallography: Single crystal X-ray structural analyses were carried out on a Rigaku Supernova diffractometer using microfocus Mo-Kα (**tPY-Me**) and Cu-Kα (**tAP**) radiation monochromatized with multi-layered optics accordingly. The structural data were deposited with CCDC. Deposition numbers 2039986, 2039983, 2039985 and 2039984 were assigned to **tAP** (dark), **tAP** (green), **tPY-Me** (plate) and **tPY-Me** (needle) accordingly. Rigaku XtaLAB PRO MM007 diffractometer with graphite monochromated Mo-Kα radiation was used for **PY-Me** (orange). The structure was solved by direct methods and expanded using Fourier techniques. Non-hydrogen atoms were refined anisotropically. Hydrogen atoms were refined using the riding model. All calculations were performed using the Olex2 crystallographic software package except for refinement, which was performed using SHELXL-2018. CIF data was confirmed by using the checkCIF/PLATON service. Powder XRD patterns were recorded on a Bruker D2 PHASER with a Si single crystal plate (Co tube, λ = 1.79026 Å). Simulated powder patterns were generated with Mercury 4.2.0 from the structures determined by the single-crystal diffraction analyses. Hirshfeld analyses were performed using CrystalExplorer version 17.5.

DSC measurements: Powder samples were sealed in an airtight capsules (15 µL vol.) and measured on a TA Instruments DSC25 discovery series with a refrigerated cooling system RCS90.

Acknowledgements

We would like to appreciate Prof. Hajime Ito (Hokkaido University), Dr. Tomohiro Seki (Hokkaido University) for single crystal X-ray analyses, and Dr. Oleksandr Pasko (SATIE UMR CNRS) for powder X-ray diffraction measurements. Y. H. gratefully acknowledges support from the Japan Society of the Promotion of Science (JSPS). R.M. and C. A. acknowledge ERC funding 'MECHANOFLUO' (St-G 715757) project.

Keywords: fluorescence • pyrene • organic materials • mechanofluorochromism • solid state emission

[1] Y. Sagara, T. Kato, *Nat. Chem.* **2009**, *1*, 605–610.
[2] Z. Chi, X. Zhang, B. Xu, X. Zhou, C. Ma, Y. Zhang, S. Liu, J. Xu, *Chem. Soc. Rev.* **2012**, *41*, 3878–3896.
[3] Y. Sagara, S. Yamane, M. Mitani, C. Weder, T. Kato, *Adv. Mater.* **2016**, *28*, 1073–1095.
[4] H. Ito, T. Saito, N. Oshima, N. Kitamura, S. Ishizaka, Y. Hinatsu, M. Wakeshima, M. Kato, K. Tsuge, M. Sawamura, *J. Am. Chem. Soc.* **2008**, *130*, 10044–10045.
[5] H. Ito, M. Muromoto, S. Kurenuma, S. Ishizaka, N. Kitamura, H. Sato, T. Seki, *Nat. Commun.* **2013**, *4*, 1–5.
[6] T. Seki, Y. Takamatsu, H. Ito, *J. Am. Chem. Soc.* **2016**, *138*, 6252–6260.
[7] Y. Sagara, T. Mutai, I. Yoshikawa, K. Araki, *J. Am. Chem. Soc.* **2007**, *129*, 1520–1521.
[8] Y. Ooyama, Y. Harima, *J. Mater. Chem.* **2011**, *21*, 8372–8380.
[9] S. Yagai, S. Okamura, Y. Nakano, M. Yamauchi, K. Kishikawa, T. Karatsu, A. Kitamura, A. Ueno, D. Kuzuhara, H. Yamada, T. Seki, H. Ito, *Nat. Commun.* **2014**, *5*, 4013.
[10] X. Y. Shen, Y. J. Wang, E. Zhao, W. Z. Yuan, Y. Liu, P. Lu, A. Qin, Y. Ma, J. Z. Sun, B. Z. Tang, *J. Phys. Chem. C* **2013**, *117*, 7334–7347.
[11] T. Wang, N. Zhang, K. Zhang, J. Dai, W. Bai, R. Bai, *Chem. Commun.* **2016**, *52*, 9679–9682.
[12] Z. Yang, Y. Zhan, Z. Qiu, J. Zeng, J. Guo, S. Hu, Z. Zhao, X. Li, S. Ji, Y. Huo, S.-J. Su, *ACS Appl. Mater. Interfaces* **2020**, *12*, 29528-29539.
[13] Z. Wang, M. Wang, J. Peng, Y. Xie, M. Liu, W. Gao, Y. Zhou, X. Huang, H. Wu, *J. Phys. Chem. C* **2019**, *123*, 27742–27751.
[14] Y. Jiang, J. Wang, G. Huang, Z. Li, B. S. Li, B. Z. Tang, *J. Mater. Chem. C* **2019**, *7*, 11790–11796.
[15] F. Liu, J. Tu, X. Wang, J. Wang, Y. Gong, M. Han, X. Dang, Q. Liao, Q. Peng, Q. Li, Z. Li, *Chem. Commun.* **2018**, *44*, 5598–5601.
[16] S. Takahashi, S. Nagai, M. Asami, S. Ito, *Mater. Adv.* **2020**, *1*, 708–719.
[17] R. Flamholc, D. Plazuk, J. Zakrzewski, R. Métivier, K. Nakatani, A. Makal, K. Woźniak, *RSC Adv.* **2014**, *4*, 31594–31601.
[18] S. K. Rajagopal, A. M. Philip, K. Nagarajan, M. Hariharan, *Chem. Commun.* **2014**, *50*, 8644–8647.
[19] D. Tchoń, D. Trzybiński, A. Wrona-Piotrowicz, A. Makal, *CrystEngComm* **2019**, *21*, 5845–5852.
[20] Y. Hirai, A. Wrona-Piotrowicz, J. Zakrzewski, A. Brosseau, R. Guillot, R. Métivier, C. Allain, *Photochem. Photobiol. Sci.* **2020**, *19*, 229–234.
[21] T. Iwasaki, S. Murakami, Y. Takeda, G. Fukuhara, N. Tohnai, Y. Yakiyama, H. Sakurai, N. Kambe, *Chem. - A Eur. J.* **2019**, *25*, 14817–14825.
[22] A. Wrona-Piotrowicz, M. Witalewska, J. Zakrzewski, A. Makal, *Beilstein J. Org. Chem.* **2017**, *13*, 1032–1038.
[23] J. Bernstein, *Polymorphism in Molecular Crystals 2e*, Oxford University Press, **2020**.
[24] M. A. Spackman, D. Jayatilaka, *CrystEngComm* **2009**, *11*, 19–32.
[25] J. J. McKinnon, M. A. Spackman, A. S. Mitchell, *Acta Crystallogr. Sect. B* **2004**, *60*, 627–668.
[26] M. A. Spackman, J. J. McKinnon, *CrystEngComm* **2002**, *4*, 378–392.
[27] L. Loots, L. J. Barbour, *CrystEngComm* **2012**, *14*, 300–304.

[28] A. Makal, J. Krzeszczakowska, R. Gajda, *Molecules* **2019**, *24*, 1–18.
[29] T. Seki, K. Kashiyama, H. Ito, *Dalt. Trans.* **2019**, *48*, 7105–7109.
[30] B. Wang, Z. Wu, B. Fang, M. Yin, *Dye. Pigment.* **2020**, *182*, 108618.
[31] V. C. Wakchaure, K. C. Ranjeesh, Goudappagouda, T. Das, K. Vanka, R. Gonnade, S. S. Babu, *Chem. Commun.* **2018**, *54*, 6028–6031.
[32] E. Nagata, S. Takeuchi, T. Nakanishi, Y. Hasegawa, Y. Mawatari, H. Nakano, *ChemPhysChem* **2015**, *16*, 3038–3043.
[33] G. Li, Y. Xu, W. Zhuang, Y. Wang, *RSC Adv.* **2016**, *6*, 84787–84793.

10.1002/cphc.202100294

WILEY-VCH

Entry for the Table of Contents (Please choose one layout)

Layout 1:

FULL PAPER

Acetyl pyrenes and pyrenyl ynones with varied molecular arrangements showed distinct emission property change upon mechanical stimuli, so-called mechanofluorochromism. The direction of emission color change as well as the spontaneous solid-state back reaction depend on the packing motifs and the steric hindrance of the side groups.

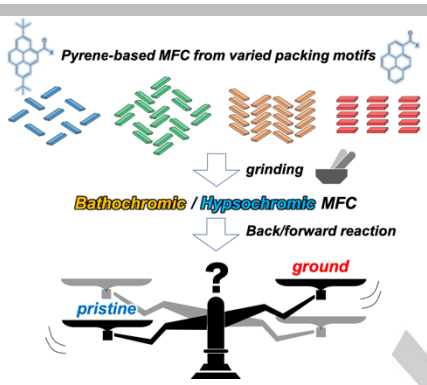

Yuichi Hirai, Lucie Laize-Générat, Anna Wrona-Piotrowicz, Janusz Zakrzewski, Anna Makal, Arnaud Brosseau, Laurent Michely, Davy-Louis Versace, Clémence Allain* and Rémi Métivier**

Page No. – Page No.

Multi-Directional Mechanofluorochromism of Acetyl Pyrenes and Pyrenyl Ynones